

# Temperature-dependent Fermi surface evolution in heavy fermion CeIrIn<sub>5</sub>

Hong Chul Choi<sup>1</sup>, B. I. Min<sup>1</sup>, J. H. Shim<sup>1,2</sup>, K. Haule<sup>3</sup>, and G. Kotliar<sup>3</sup>

<sup>1</sup>*Department of Physics, Pohang University of Science and Technology, Pohang 790-784, Korea*

<sup>2</sup>*Department of Chemistry, Pohang University of Science and Technology, Pohang 790-784, Korea and*

<sup>3</sup>*Department of Physics, Rutgers University, Piscataway, NJ 08854, USA*

(Dated: October 18, 2018)

PACS numbers: 71.18.+y, 71.27.+a, 72.15.Qm

In Cerium-based heavy electron materials, the  $4f$  electron's magnetic moments bind to the itinerant quasiparticles to form composite heavy quasiparticles at low temperature ( $T$ ). The volume of the Fermi surface (FS) in the Brillouin zone incorporates the moments to produce a "large FS" due to the Luttinger theorem. When the  $f$  electrons are localized free moments, a "small FS" is induced since it contains only broad bands of conduction  $spd$  electrons. We have addressed theoretically the evolution of the heavy fermion FS as a function of  $T$ , using a first principles dynamical mean-field theory (DMFT) approach combined with density functional theory (DFT+DMFT). We focus on the archetypical heavy electrons in CeIrIn<sub>5</sub>, which is believed to be near a quantum critical point. Upon cooling, both the quantum oscillation frequencies and cyclotron masses show logarithmic scaling behavior ( $\sim \ln(T_0/T)$ ) with different characteristic temperatures  $T_0 = 130$  and  $50$  K, respectively. The enlargement of the electron FS's at low  $T$  is accompanied by topological changes around  $T = 10 \sim 50$  K. The resistivity coherence peak observed at  $T \simeq 50$  K is the result of the competition between the binding of incoherent  $4f$  electrons to the  $spd$  conduction electrons at Fermi level ( $E_F$ ) and the formation of coherent  $4f$  electrons.

The FS volume has been a sensitive probe of the character, localized or itinerant, of the heavy fermion system.<sup>1</sup> Intensive efforts have been devoted to the study of the quantum phase transition leading from a small to large FS at strictly zero temperature. While the FS, as a surface of discontinuity in the momentum distribution function, is sharply defined only at zero temperature, experimental probes such as the angle-resolved photoemission spectra (ARPES) and magnetic quantum oscillation experiments such as de Haas-van Alphen (dHvA) or Shubnikov-de Haas experiments identify the region of momentum space where zero energy fermionic excitations exist at finite temperature. ARPES experiment directly observes the FS in the momentum space. But, high resolution is required to determine the FS size. The quantum oscillation experiments measure the precise value of the FS area in a specific plane by probing the oscillation frequencies of magnetization as a function of the applied magnetic field. The quantum oscillation

frequency( $F$ ), the so-called dHvA frequency, is proportional to the extremal cross-sectional area  $S_F$  of the FS ( $F = \hbar S_F / 2\pi e$ ). The quantum oscillation experiments also provide the information on the cyclotron effective electron mass  $m^* (= (\hbar^2 / 2\pi) \partial S_F / \partial \omega)$  and the geometry of the FS's.

The band structure calculation is a complementary tool to the quantum oscillation experiment to analyze the complicated FS of the multiple band system. Quantum oscillation frequencies of heavy fermion materials, such as CeCu<sub>6</sub>, UPt<sub>3</sub>, and Ce(Ir,Co)In<sub>5</sub>, are explained well by conventional band calculations because the itinerant  $4f$  electrons behave as conduction electrons near  $E_F$ . Although the geometry and volume of FS's are well explained by the DFT band calculation, the detected cyclotron mass  $m^*$  is much larger than the corresponding DFT band mass  $m_b$ ,<sup>2-5</sup> because the DFT calculation can not describe the correlated  $4f$  electronic states correctly. When the  $4f$  electrons are localized in the antiferromagnetic (AFM) compounds, such as CeRhIn<sub>5</sub>, CeIn<sub>3</sub>, CeRh<sub>2</sub>Si<sub>2</sub>, the  $4f$ -localized band model is more applicable to the description of the quantum oscillation experiments.<sup>2,5</sup> The  $4f$ -localized band model can be performed by treating the  $4f$  electrons as core within the DFT (open-core DFT) band calculation,<sup>2</sup> or by employing the DFT+ $U$  band method ( $U$ : on-site Coulomb interaction).<sup>7</sup>

CeTIn<sub>5</sub> ( $T = \text{Co, Rh, and Ir}$ ) has been a prototypical system to study the crossover behavior between the itinerant and localized  $4f$  electrons. CeCoIn<sub>5</sub><sup>8</sup> and CeIrIn<sub>5</sub><sup>9</sup> have itinerant  $4f$  electrons and superconducting ground states at low  $T$ . On the other hand, CeRhIn<sub>5</sub> has localized  $4f$  electrons and the AFM ground state. The measured dHvA frequency of each compound identifies the nature of Ce  $4f$  electrons, whether they are itinerant or localized. CeCoIn<sub>5</sub><sup>2,4,6</sup> and CeIrIn<sub>5</sub><sup>2,3</sup> have enlarged electron FS's due to the contribution of itinerant  $4f$  electrons, while CeRhIn<sub>5</sub> has similar geometry of FS's but smaller size of FS's.<sup>2,5</sup> For CeRhIn<sub>5</sub>, pressure-induced superconductivity was observed for  $P > 1.63$  GPa,<sup>10</sup> and the drastic change in the FS was detected at a critical pressure of  $P_c \simeq 2.35$  GPa.<sup>11</sup> On the other hand, CeRh<sub>1-x</sub>Co<sub>x</sub>In<sub>5</sub> shows the the doping-dependent reconstruction of FS deep inside the magnetically ordered state,<sup>12</sup> away from the quantum critical point. The  $T$ -dependent evolution between itinerant and localized electrons also has been described by the phenomenological

two-fluid model, where the universal scaling behavior can be applied to various physical properties of the heavy fermion compounds.<sup>13–15</sup>

In this Letter, we have addressed the  $T$ -dependent crossover from localized to itinerant  $4f$  electrons in CeIrIn<sub>5</sub>, and investigated its effects on the FS properties and electrical resistivity. The charge self-consistent version of DFT+DMFT approach,<sup>16</sup> as implemented in Ref.17, is based on the full-potential linearized augmented plane-wave (FP-LAPW) band method.<sup>18</sup> The correlated  $4f$  electrons are treated dynamically by the DMFT local self-energy, while all other delocalized  $spd$  electrons are treated on the DFT level. The local self-energy matrix  $\Sigma(\omega)$  is calculated from the corresponding impurity problem, in which full atomic interaction matrix is taken into account.<sup>19</sup> To solve the impurity problem, we use both the vertex corrected one-crossing approximation<sup>16</sup> and the continuous time quantum Monte-Carlo method.<sup>20,21</sup>

The main difference between low and high  $T$  spectral functions in the DFT+DMFT calculation is the existence of  $4f$  bands near  $E_F$ , as shown in Supplementary Fig. 1. Ce  $4f$  bands at high  $T$  are absent near  $E_F$ , and their spectral weights are distributed into the lower and upper Hubbard bands. The spectral function near  $E_F$  can be well described by the quasiparticle band structures of other  $spd$  electrons although there is a small scattering rate due to the hybridization between the conduction electrons at  $E_F$  and the incoherent Ce  $4f$  electrons in the Hubbard bands. As decreasing  $T$ , the spectral weight of the renormalized Ce  $4f$  bands is increased continuously (see Supplementary Movie 1.). The hybridization of the  $4f$  and other  $spd$  bands produces very massive almost flat quasiparticle band structures near  $E_F$ . These flat bands emerge as the narrow Kondo peak at  $E_F$  in the photoemission spectra.<sup>22</sup>

The  $T$ -dependent FS has been extracted from the quasiparticle band structures. At low  $T$ , the FS's of the DFT+DMFT calculation are very similar to those of the DFT calculation, as shown in Fig. 1. Upon heating, the Ce  $4f$  electrons become localized and their contribution to  $E_F$  is suppressed. Accordingly, the areas of electron FS's ( $\alpha_i$  and  $\beta_i$ ) are continuously decreased. In contrast, there occur rather big changes in other FS's areas upon heating. The areas of the  $g$  and  $h$  hole FS's on the  $z = 0$  plane grow and merge into one closed electron FS. The  $a$  electron FS identified at  $T = 10$  K on the  $z = \pi$  plane is divided at high  $T$ , and so new hole FS's appear near Z and R symmetry points. The continuous  $T$ -dependent evolution of the FS is provided in Supplementary Movie 2. By integrating the volume of electron FS's, the occupancy of the conduction electrons has been counted. It shows the continuous change from 3 to 4 electrons as temperature is decreased, which reflects the participation of one Ce  $4f$  electron in the bonding.

Because the area of the FS is directly related to the size of the  $4f$  electron contribution to  $E_F$ , we have investigated the  $T$ -dependent dHvA frequencies, as shown

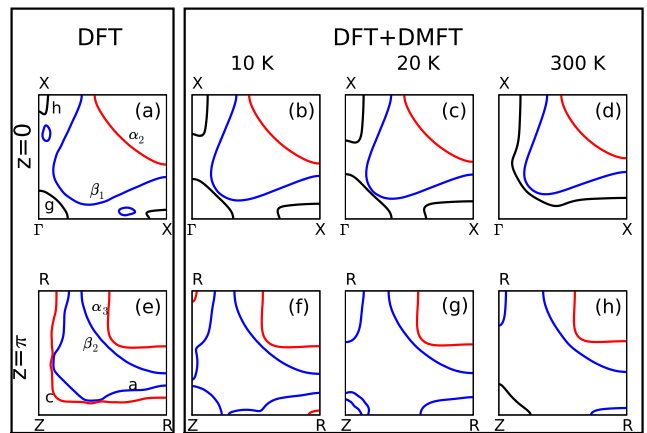


FIG. 1: **The  $T$ -dependent FS evolution in the DFT+DMFT calculation.** The FS's are extracted from the DFT+DMFT quasiparticle band structures at 10 K(b,f), 20 K(c,g) and 300 K(d,h). For comparison, the FS's obtained from the DFT band calculation are also provided (a,e). Because the main FS's in CeIrIn<sub>5</sub> are nearly cylindrical due to the quasi-2D nature of its crystal structure, the FS's only on the  $z = 0$  and  $z = \pi$  planes are shown. The FS's on these planes are identified from the dHvA frequencies because the symmetric plane provides the extremal cross-section of the FS. There are two main cylindrical electron FS's represented by  $\alpha_i$  and  $\beta_i$  branches observed in the dHvA experiment (see (a) and (e)). Those branches are identified at all temperature range. On the other hand, the FS's denoted as  $g, h$  (hole FS's) and  $a, c$  (electron FS's) in the DFT calculation manifest topological changes with varying  $T$  in the DFT+DMFT calculation. Note that  $g, h, a, c$  branches were not identified clearly in the dHvA experiments. Color represents the different band index.

in Fig. 2(a). At high  $T$ , the dHvA frequencies are well consistent with those from the Ce  $4f$  open-core DFT calculation. With decreasing  $T$ , they show the continuous increase with the participation of  $4f$  electrons to  $E_F$  and follow the scaling behavior of  $\ln(T_0/T)$ , as shown in Fig. 2(c). All the branches show the same characteristic temperature  $T_0^f \sim 130$  K. This behavior is consistent with the increase of the number of conduction electrons with decreasing  $T$ .

The cyclotron mass corresponds to the effective mass of the carriers at the specific FS. As shown in Fig. 2(b) and (d), the calculated cyclotron masses also increase upon cooling, and follow a similar scaling behavior of  $\sim \ln(T_0/T)$  with  $T_0^m \sim 50$  K. The cyclotron masses are also well fitted by the description of two fluid model by Yang *et al.*<sup>14</sup>:  $(1 - T/T_0)^{3/2}[1 + \ln(T_0/T)]$  with same  $T_0^m \sim 50$  K. Interestingly,  $T_0^m$  is coincident with the coherent temperature  $T^*$  of Ce  $4f$  states,<sup>22</sup> but clearly different from  $T_0^f$ . This feature reveals the  $4f$  electrons start to participate in bonding through the hybridization with  $spd$  electrons at the temperature scale  $T_0^f$ , which is higher than the temperature  $T_0^m$  at which the coherent heavy fermion electronic states are formed. These results are reminis-

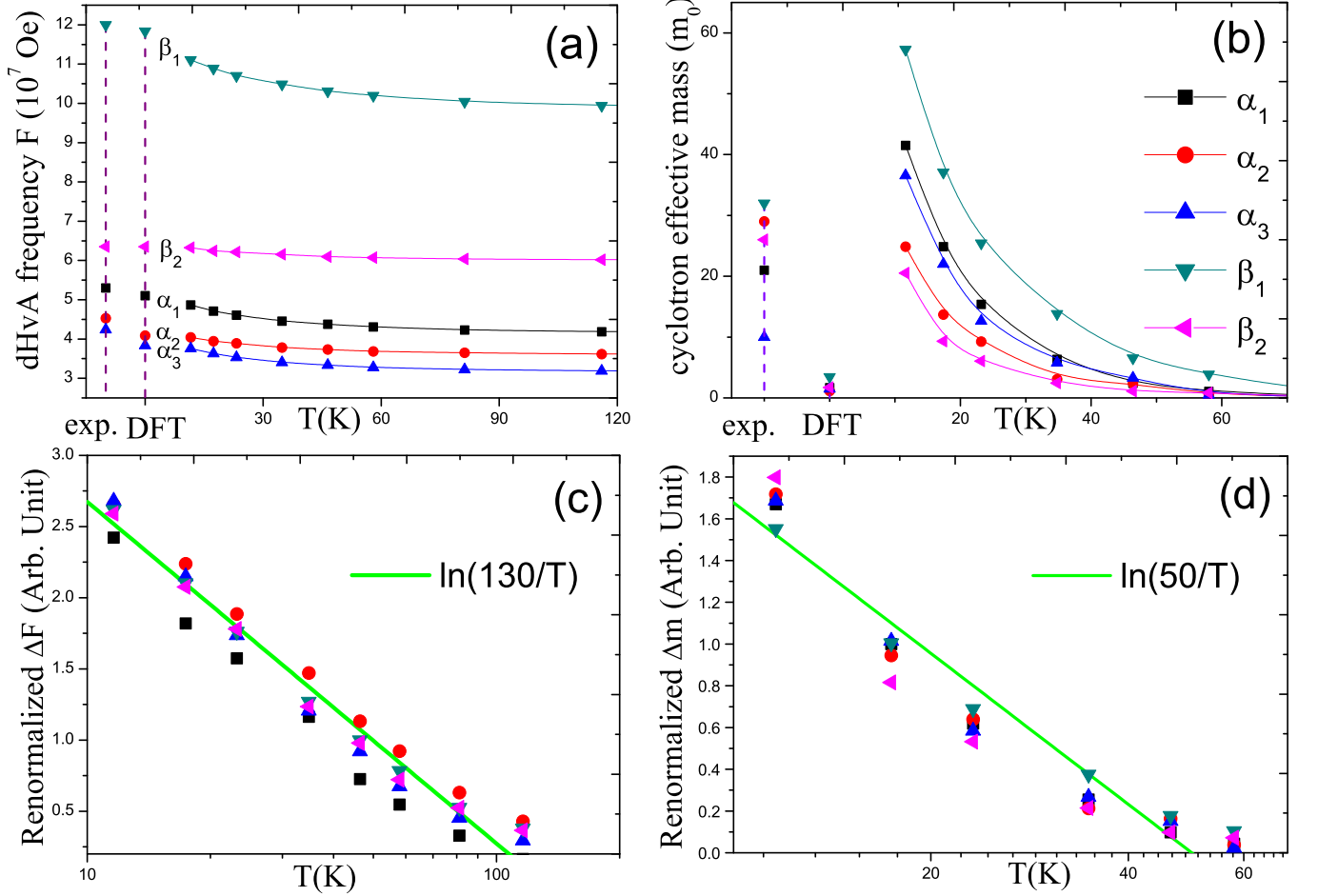


FIG. 2: **The  $T$ -dependent dHvA frequencies ( $F$ ) and cyclotron effective masses ( $m^*$ ).** The dHvA frequencies (a) and effective masses (b) of  $\alpha_i$  and  $\beta_i$  branches are obtained from the DFT+DMFT method, and compared with those from the DFT method and experiments (exp). The corresponding FS's for each branch are provided in Fig. 1(a,e), except  $\alpha_1$  that corresponds to the maximum frequency among  $\alpha_i$  branches and is located between the  $z = 0$  and  $z = \pi$  planes. At high  $T$ , the cyclotron masses are very small, ranging from 0.4 to 0.7  $m_0$  ( $m_0$ : bare electron mass) for  $\alpha_i$  and  $\beta_i$  branches. Such small cyclotron masses are also reproduced in the  $4f$  open-core DFT calculation, in which only dispersive *spd* bands are crossing  $E_F$ . The low  $T$  dHvA frequencies from the DFT+DMFT method are consistent with the results of DFT method in which the  $4f$  electrons are considered as itinerant type. (c) The renormalized  $\Delta F_i$  of each branch shows the scaling behavior of  $\ln(T_0^f/T)$  with the characteristic  $T$  of  $T_0^f \sim 130$  K. (d) All the renormalized  $\Delta m^*$ 's show the similar scaling behavior, but with  $T_0^m \sim 50$  K.

cent of recent experiment, which shows the occurrence of FS reconstruction much earlier than the quantum critical transition.<sup>12</sup> Note that the above scaling law is consistent with the two-fluid model,<sup>14</sup> in which the coherent  $4f$  bands start to grow below  $T^*$ .

All the calculated cyclotron masses at  $T = 10$  K seem to be overestimated with respect to the experimental values<sup>3</sup> roughly by a factor of two. It is well known that the value of cyclotron mass has a substantial dependence on the applied magnetic field.<sup>4</sup> In the presence of the magnetic field, the effective mass can be reduced by the change of the hybridization, even without much change of the FS geometry.<sup>23</sup> If one considers the high magnetic field in experiments, the calculated cyclotron masses would be consistent with experimental values at

low  $T$ .

The continuous change of FS properties with  $T$  variation is deeply related to the transport properties. Figure 3 (a) provides the calculated resistivity for CeIrIn<sub>5</sub> as a function of  $T$ , which is compared to the experimental electrical resistivity. The electrical resistivity is calculated using the real part of the dc conductivity ( $\sigma$ )<sup>17</sup> based on the DFT+DMFT spectral function near  $E_F$ : 
$$\sigma^{\mu\nu} = \frac{\pi e^2}{V} \sum_{\mathbf{k}} \int d\omega \left( -\frac{df}{d\omega} \right) \text{Tr} [A(\mathbf{k}, \omega) v^{\mathbf{k}\mu} A(\mathbf{k}, \omega) v^{\mathbf{k}\nu}].$$
 Here  $\mu$  and  $\nu$  represent spatial coordinates.  $V$ ,  $f(\omega)$ , and  $v$  are the primitive volume, the Fermi Dirac distribution function, and the velocity, respectively. The calculated resistivities from low to high  $T$  are in good agreement with the experimental resistivity. At high  $T$ , the elec-

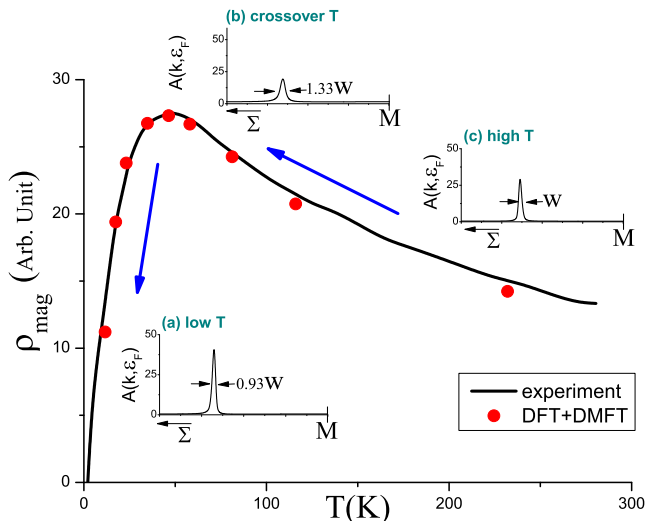


FIG. 3: **The magnetic part ( $4f$  electron contribution) of the resistivity as a function of  $T$ .** The experimental electrical resistivity is obtained by subtracting the resistivity of  $\text{LaIrIn}_5$  from that of  $\text{CeIrIn}_5$ .<sup>5</sup> Inset Fig. (a), (b), and (c) show the broadening changes of spectral weights at  $E_F$  at low (10K), crossover (50 K), and high temperature (1000 K), respectively.  $\Sigma$  means the direction from  $M$  to  $\Gamma$  in momentum space.

tronic carriers from dispersive  $spd$  bands become more and more decoupled from localized electrons in the  $4f$  shell, hence the carriers are scattered less at very high  $T$ . Upon cooling, the hybridization among local moments and  $spd$  carriers increases while the  $4f$  electrons remain very incoherent above 50 K, causing enhanced scattering mechanism for electric carriers. Below the scale  $T_0^m$ , the electrons in the  $4f$  shell also gain coherence which substantially suppresses resistivity. Therefore, the maximum resistivity is observed near 50 K. Inset Fig. 3(a), (b), and (c) show the broadening of spectral weight at  $E_F$ , calculated at low, crossover, and high  $T$ , respectively. The broadening corresponds to the scattering rate at the specific  $\mathbf{k}$ -point. It is noted that the spreading of the spectral weight at crossover is wider than that at high or low  $T$ . This finding confirms that the DFT+DMFT calculation describes well the crossover behavior of Ce  $4f$  electrons with one  $T_0^f$  ( $\sim 130$  K) for the participation of  $4f$  electrons in the conduction and another  $T_0^m$  ( $\sim 50$  K) for the

formation of coherent heavy electron  $4f$  bands.

We have examined the evolution of the heavy fermion state using electronic structure methods. As in the two fluid phenomenology,<sup>13</sup> the experimental studies of other heavy fermion systems<sup>24</sup> as well as the slave boson studies,<sup>25,26</sup> the crossover from the high  $T$  regime, where moments and quasiparticles coexist, to the low  $T$  Fermi liquid heavy fermion state, has a rich structure characterized by multiple energy scales. We have found that it is characterized by multiple scales which have a clear correspondence with physical observables.  $T_0^f$  is the onset of the sharp crossover where the small FS begins distorting towards the low  $T$  FS. At a lower  $T_0^m$ , composite quasiparticles formed from  $f$ -moments and conduction electrons emerge, and this is signaled by a maximum of the resistivity. By that point, the FS has reached a shape which is closer to its zero temperature final value, but the material is not yet a Fermi liquid, which is only reached at a much lower temperature  $T_{FL}$ . We can only put bounds for this quantity as being lower than 10 K for the 115 material.

The theory can be tested using several techniques such as ARPES, Compton scattering and scanning tunnelling microscopy, which have been developed as powerful tools for exploring the evolution of the electronic structure and are currently under way.<sup>27</sup> Our theory predicts that both  $T_0^m$  and  $T_0^f$  increase as a function of pressure in the  $\text{CeIrIn}_5$  material. More generally, it would be interesting to follow these scales as a function of control parameters such as pressure and composition, to investigate the behavior of  $T_0^m$  and  $T_0^f$  in related materials which can be driven to a quantum critical point.

## Acknowledgments

We acknowledge useful discussions with Tuson Park. This work was supported by the NRF (No. 2009-0079947, 2010-0006484, 2010-0026762), WCU through KOSEF (No. R32-2008-000-10180-0), and by the POSTECH BK21 Physics Division. K. Haule was supported by Grant NSF NFS DMR-0746395 and Alfred P. Sloan fellowship. G. Kotliar was supported by NSF DMR-0906943

<sup>1</sup> Settai, R., Takeuchi, T. & Ōnuki, Y. Recent Advances in Ce-Based Heavy-Fermion Superconductivity and Fermi Surface Properties. *J. Phys. Soc. Jpn.* **76**, 051003 (2007).  
<sup>2</sup> Elgazzar, S., Opahle, I., Hayn, R. & Oppeneer, P. M. Calculated de Haas-van Alphen quantities of  $\text{CeMIn}_5$  ( $M=\text{Co}$ ,  $\text{Rh}$ , and  $\text{Ir}$ ) compounds. *Phys. Rev. B* **69**, 214510 (2004).  
<sup>3</sup> Y. Haga *et al.* Quasi-two-dimensional Fermi surfaces of the heavy fermion superconductor  $\text{CeIrIn}_5$ . *Phys. Rev. B* **63**, 060503(R) (2001).

<sup>4</sup> Settai, R., Shishido, H., Ikeda, S., Murakawa, Y., Nakashima, M., Aoki, D., Haga, Y., Harima, H. & Ōnuki, Y. Quasi-two-dimensional Fermi surfaces and the de Haas-van Alphen oscillation in both the normal and superconducting mixed states of  $\text{CeCoIn}_5$ . *J. Phys.: Condens. Matter* **13**, L627 (2001).  
<sup>5</sup> Shishido, H. *et al.* Fermi Surface, Magnetic and Superconducting Properties of  $\text{LaRhIn}_5$  and  $\text{CeTiIn}_5$  ( $T$ :  $\text{Co}$ ,  $\text{Rh}$  and  $\text{Ir}$ ). *J. Phys. Soc. Jpn.* **71**, 162 (2002).

- <sup>6</sup> Hall, D., Palm, E. C., Murphy, T. P., Tozer, S. W., Fisk, Z., Alver, U., Goodrich, R. G., Sarrao, J. L., Pagliuso, P. G. & Ebihara, T. Fermi surface of the heavy-fermion superconductor CeCoIn<sub>5</sub>: The de Haas-van Alphen effect in the normal state. *Phys. Rev. B* **64**, 212508 (2001).
- <sup>7</sup> Wang, J. L., Zeng, Z., Zheng, Q. Q. & Lin, H. Q. Electronic structure of heavy fermion superconductor CeMIn<sub>5</sub> (M=Co,Rh,Ir). *J. Appl. Phys.* **93**, 6891 (2003).
- <sup>8</sup> Petrovic, C., Pagliuso, P. G., Hundley, M. F., Movshovich, R., Sarrao, J. L., Thompson, J. D., Fisk, Z. & Monthoux, P. Heavy-fermion superconductivity in CeCoIn<sub>5</sub> at 2.3 K. *J. Phys. Cond. Matt.* **13**, L337 (2001).
- <sup>9</sup> Petrovic, C., Movshovich, R., Jaime, M., Pagliuso, P. G., Hundley, M. F., Sarrao, J. L., Fisk, Z. & Thompson, J. D. A new heavy-fermion superconductor CeIrIn<sub>5</sub>: A relative of the cuprates? *Europhys. Lett.* **53**, 354 (2001).
- <sup>10</sup> Hegger, H., Petrovic, C., Moshopoulou, E. G., Hundley, M. F., Sarrao, J. L., Fisk, Z. & Thompson, J. D. Pressure-Induced Superconductivity in Quasi-2D CeRhIn<sub>5</sub>. *Phys. Rev. Lett.* **84**, 4986 (2000).
- <sup>11</sup> Shishido, H., Settai, R., Harima, H. & Ōnuki, Y. A Drastic Change of the Fermi Surface at a Critical Pressure in CeRhIn<sub>5</sub>: dHvA Study under Pressure. *Phys. Soc. Jpn.* **74**, 1103 (2005).
- <sup>12</sup> Goh, S. K., Paglione, J., Sutherland, M., O'Farrell, E. C. T., Bergemann, C., Sayles, T. A., & Maple, M. B. Fermi-surface reconstruction in CeRh<sub>1-x</sub>Co<sub>x</sub>In<sub>5</sub>. *Phys. Rev. Lett.* **101**, 056402 (2008).
- <sup>13</sup> Nakatsuji, S., Pines, D. & Fisk, Z. Two Fluid Description of the Kondo Lattice. *Phys. Rev. Lett.* **92**, 016401 (2004).
- <sup>14</sup> Yang, Y.-f. & Pines, D. Universal Behavior in Heavy-Electron Materials. *Phys. Rev. Lett.* **100**, 096404 (2008).
- <sup>15</sup> Yang, Y.-f., Fisk, Z., Lee, H.-O., Thompson, J. D. & Pines, D. Scaling the Kondo lattice *Nature* **454**, 611 (2008).
- <sup>16</sup> Kotliar, G., Savrasov, S. Y., Haule, K., Oudovenko, V. S., Parcollet, O. & Marianetti, C. A. Electronic structure calculations with dynamical mean-field theory. *Rev. Mod. Phys.* **78**, 865 (2006).
- <sup>17</sup> Haule, K., Yee, C.-H. & Kim, K. Dynamical mean-field theory within the full-potential methods: Electronic structure of CeIrIn<sub>5</sub>, CeCoIn<sub>5</sub>, and CeRhIn<sub>5</sub>. *Phys. Rev. B* **81**, 195107 (2010).
- <sup>18</sup> Blaha, P., Schwarz, K., Madsen, G., Kvasnicka, D. & Lutz, J. in *Wien2K*, edited by K. Schwarz (Technische Universitat Wien, Austria, 2001).
- <sup>19</sup> Cowan, R. D. *The Theory of Atomic Structure and Spectra* (Univ. California Press, Berkeley, 1981).
- <sup>20</sup> Haule, K. Quantum Monte Carlo impurity solver for cluster dynamical mean-field theory and electronic structure calculations with adjustable cluster base. *Phys. Rev. B* **75**, 155113 (2007).
- <sup>21</sup> Werner, P., Comanac, A., de'Medici, L., Troyer, M. & Millis, A. J. Continuous-Time Solver for Quantum Impurity Models. *Phys. Rev. Lett.* **97**, 076405 (2006).
- <sup>22</sup> Shim, J. H., Haule, K., Kotliar, G. Modeling the Localized-to-Itinerant Electronic Transition in the Heavy Fermion System CeIrIn<sub>5</sub>. *Science* **318**, 1615 (2007).
- <sup>23</sup> Ebihara, T., Bauer, E. D., Cornelius, A. L., Lawrence, J. M., Harrison, N., Thompson, J. D. Sarrao, J. L., Hundley, M. F. & Uji, S. Dependence of the Effective Masses in YbAl<sub>3</sub> on Magnetic Field and Disorder. *Phys. Rev. Lett.* **90**, 166404 (2003).
- <sup>24</sup> Gegenwart, P., Westerkamp, T., Krellner, C., Tokiwa, Y., Paschen, S., Geibel, C., Steglich, F., Abrahams, E. & Si, Q. Multiple Energy Scales at a Quantum Critical Point. *Science* **315**, 969 (2007).
- <sup>25</sup> Burdin, S. & Zlatić, V. Multiple temperature scales of the periodic Anderson model: Slave boson approach. *Phys. Rev. B* **79**, 115139 (2009).
- <sup>26</sup> Burdin, S., Georges, A. & Grepel, D. R. Coherence scale of the Kondo lattice. *Phys. Rev. Lett* **85**, 1048 (2000).
- <sup>27</sup> Delinger, J. D. *et al.* private communications.

# Temperature dependent Fermi surface evolution in heavy fermion CeIrIn<sub>5</sub> -Supplementary Information-

Hong Chul Choi<sup>1</sup>, B. I. Min<sup>1</sup>, J. H. Shim<sup>1,2</sup>, K. Haule<sup>3</sup>, and G. Kotliar<sup>3</sup>

<sup>1</sup>*Department of Physics, Pohang University of Science and Technology, Pohang 790-784, Korea*

<sup>2</sup>*Department of Chemistry, Pohang University of Science and Technology, Pohang 790-784, Korea and*

<sup>3</sup>*Department of Physics, Rutgers University, Piscataway, NJ 08854, USA*

(Dated: October 18, 2018)

PACS numbers: 71.18.+y, 71.27.+a, 72.15.Qm

## I. SPECTRAL FUNCTION ( $A(k, \omega)$ )

The main difference between the conventional DFT band structure and the Ce  $4f$ -localized (open-core) DFT band structure is the existence of  $4f$  bands near  $E_F$ , as shown in Supplementary Fig. 1 (blue lines). In the DFT band structure in Supplementary Fig. 1(a), one can notice the spin-orbit (SO) split  $j = 5/2$  and  $7/2$  states of Ce  $4f$  flat bands, which are located around 0.3 and 0.6 eV, respectively (clearly distinguishable at M and A). They are hybridized with other conduction ( $spd$ ) bands to form dispersive bands near  $E_F$ . Three bands containing Ce  $4f$  ( $j = 5/2$ ) states are crossing  $E_F$ , and the occupancy of these bands is counted to four electrons: three  $spd$  electrons and one Ce  $4f$  electron. On the other hand, in the  $4f$  open-core DFT band structure in Supplementary Fig. 1(b), there is no contribution from Ce  $4f$  electrons and only dispersive  $spd$  bands are observed. The occupancy of these bands is counted to three electrons due to the absence of one  $4f$  electron.

We have also provided the DFT+DMFT spectral functions obtained at low ( $T = 10$  K) and high ( $T = 300$  K) temperature. It is seen in Supplementary Fig. 1(b) that Ce  $4f$  bands at high  $T$  are completely removed from  $E_F$ , and their spectral weights are redistributed into lower and upper Hubbard bands at -2.5 eV and +3 eV (not shown here). The spectral function near  $E_F$  can be well described by the quasi-particle band structures of  $spd$  electrons only, although there is small scattering rate due to the hybridization between conduction electrons at  $E_F$

and incoherent Ce  $4f$  electrons at the Hubbard bands. Noteworthy is that the quasi-particle  $spd$  bands near  $E_F$  are very similar to those of the  $4f$  open-core DFT band calculation.

At low  $T$  in Supplementary Fig. 1 (a), the DFT+DMFT spectral functions near  $E_F$  have quasi-particle band structures of Ce  $4f$  ( $j=5/2$ ) states that are hybridized with  $spd$  states. The bandwidth of Ce  $4f$  ( $j=5/2$ ) states is about 3 meV, which is  $\sim 1/100$  smaller than that obtained in the DFT band calculation. That is why they are shown as straight lines in this narrow energy range. The renormalized Ce  $4f$  bands are hybridized with other  $spd$  bands to produce flat quasi-particle band structures, as shown in Supplementary Fig. 1(a). These flat bands emerge as the narrow Kondo peak at  $E_F$  in the photoemission spectra. Because Ce  $4f$  ( $j=5/2$ ) states are simply renormalized with respect to  $E_F$ , the quasi-particle bands reproduce the FS's of the DFT band calculation.

## II. THE CONTINUOUS $T$ -DEPENDENT IMAGES OF THE SPECTRAL FUNCTIONS

The images for moving pictures (Movies 1 and 2) are provided for the additional Supplementary information. Movie 1 shows the  $T$ -dependent variation of  $A(k, \omega)$  on the  $\mathbf{k}$ -points between  $\Gamma$  and  $X$  from  $T = 10$  to 1000 K. The Movie 2 demonstrates the  $T$ -dependent variation of FS's on the  $z = 0$  plane from  $T = 10$  to 1000 K.

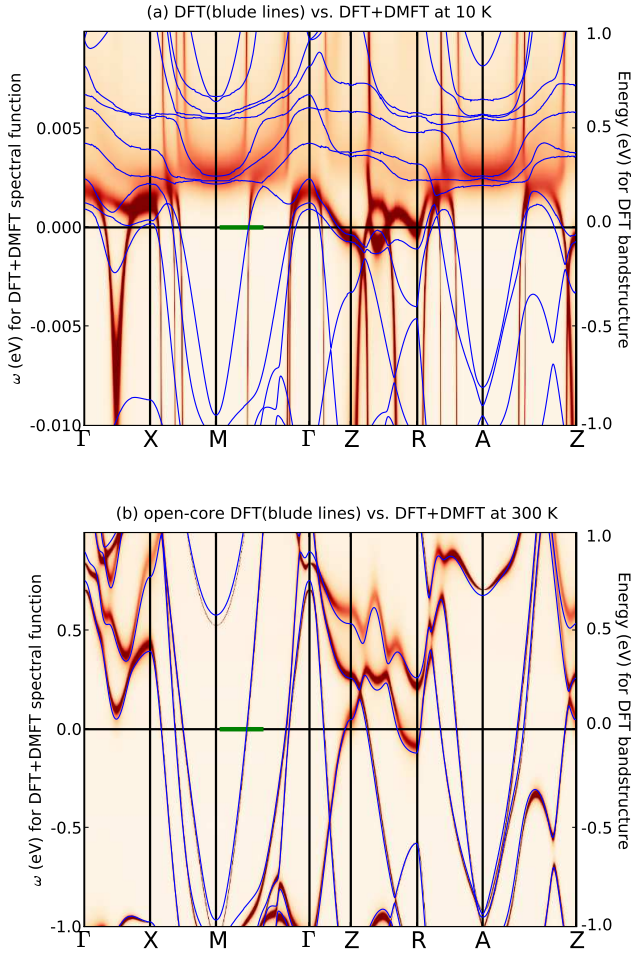


**FIG. 1: The DFT band structures and DFT+DMFT spectral functions at high and low  $T$ .** The DFT+DMFT spectral functions calculated at  $T = 10$  K (a) and 300 K (b) along the symmetry lines are provided. The spectral function  $A(k, \omega)$  is obtained from  $A(k, \omega) = -\frac{1}{\pi} \text{Im}G(k, \omega)$ . In (a), the DFT band structures, in which Ce  $4f$  electrons are treated as valence electrons (delocalized limit), are drawn with blue lines. In (b), the  $4f$  open-core DFT band structures, in which Ce  $4f$  electrons are treated as core electrons (localized limit), are drawn with blue lines. The green lines along M and  $\Gamma$  indicate the  $\mathbf{k}$ -point paths used in Inset Fig. 3 (a), (b), and (c) of the Letter.